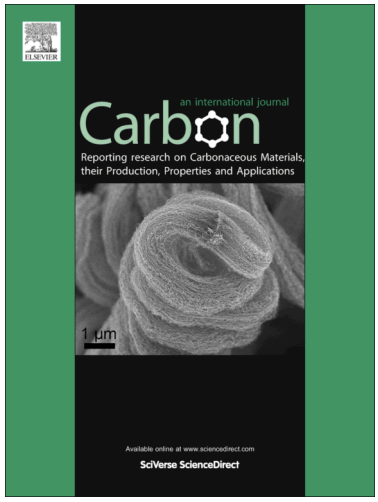

Buckling of ZnS-filled single-walled carbon nanotubes – the influence of aspect ratio

André O. Monteiro, Pedro M.F.J. Costa, Paulo B. Cachim, David Holec

PII: S0008-6223(14)00751-9
DOI: http://dx.doi.org/10.1016/j.carbon.2014.08.011
Reference: CARBON 9220

To appear in: *Carbon*

Received Date: 18 February 2014
Accepted Date: 7 August 2014

Please cite this article as: Monteiro, A.O., Costa, P.M.F., Cachim, P.B., Holec, D., Buckling of ZnS-filled single-walled carbon nanotubes – the influence of aspect ratio, *Carbon* (2014), doi: http://dx.doi.org/10.1016/j.carbon.2014.08.011

Buckling of ZnS-filled single-walled carbon nanotubes – the influence of aspect ratio

André O. Monteiro[a,b,*], Pedro M. F. J. Costa[c,d], Paulo B. Cachim[b,e], David Holec[f]

[a] CICECO, University of Aveiro, 3810-193 Aveiro, Portugal

[b] Department of Civil Engineering, University of Aveiro, 3810-193 Aveiro, Portugal

[c] Physical Sciences and Engineering Division, KAUST, 23955-6900 Thuwal, Kingdom of Saudi Arabia

[d] Department of Materials and Ceramic Engineering, University of Aveiro, 3810-193 Aveiro, Portugal

[e] LABEST, University of Aveiro, 3810-193 Aveiro, Portugal

[f] Department of Physical Metallurgy and Materials Testing, Montanuniversität Leoben, 8700 Leoben, Austria

Dedicated to Prof. Maria José Calhorda on occasion of her 65th birthday.

Abstract

The mechanical response of single-walled carbon nanotubes (SWCNT) filled with crystalline zinc sulphide (ZnS) nanowires under uniaxial compression is studied using classical molecular dynamics. These simulations were used to analyse the behaviour of SWCNT, with and without ZnS filling, in terms of critical force and critical strain. Force versus strain curves have been computed for hollow and filled systems, the latter clearly showing an improvement of the mechanical behaviour caused by the ZnS nanowire. The same simulations were repeated for a large range of dimensions in order to evaluate the influence of the aspect ratio on the mechanical response of the tubes.

1. Introduction

Filling the cavities of carbon nanotubes generates new hybrid materials, an approach that can lead to the customisation and/or improvement of physical properties of either the host nanotube or the guest encapsulated substance [1]. The first record describing these host-guest systems dates back to 1993 [2], when the encapsulation of lead/lead oxide within multi-walled carbon nanotubes (MWCNT) was performed using the so-called "capillary method". Till present days, hundreds of

[*] Corresponding author. Tel: (+351) 927 852 316. E-mail address: andre.monteiro@ua.pt (André Monteiro)

these systems have been produced with the prospect for applications spanning from drug delivery [3-6] to storage of sensitive materials [7] and nanopipetting [8, 9].

Recently, we have been studying a relatively complex system which is composed of a ternary alloy guest, Ga-doped ZnS, confined in turbostratic MWCNT, for electrically-activated nanodelivery [8, 10]. Besides characterising its structure and chemistry, we have also analysed the reactivity [11], thermal stability [12, 13] and mechanical behaviour [14-17]. Note that this work was carried out at the discrete nanostructure level providing therefore a more detailed view of the material's behaviour than the averaged responses obtained from bulk samples [18]. Such an approach is particularly relevant for mechanical studies where the heterogeneity of bulk samples (in terms of orientation, diameter range…) influences considerably the outcome of force-displacement measurements. Accordingly, we have demonstrated how the stiffness of the host MWCNT is altered by the inclusion of the guest II-VI semiconductor [19]. As a next logical step, we developed a computational model that helps understanding the mechanics of this hybrid material [15]. In the first stage, we adopted an approach based on finite elements as it allowed handling the correct dimensions of the (doped-)ZnS@MWCNT system (here, @ means "encapsulated in"). In this model, a fully rigid platelet was included at each end to account for the clamps, one of which acted as the force sensor and the other as the displacement actuator. The displacement was applied according to the longitudinal axis of the CNT. Overall, both the experimental behaviour and force-displacement curves could be reproduced. Whilst the continuum approach is appropriate for the present system, it has considerable limitations in regards to structures with smaller dimensions, such as SWCNTs [20]. Given our interest in nanodelivery it would be useful to extend this confined semiconductor system to the single-walled case as one can deposit within ever smaller amounts of ZnS. Furthermore, following the effect of filling in the mechanical properties of Zn(Ga)S@MWCNT [14], the stiffness may be used as a marker for the filled vs. empty states without having to resort to sophisticated electron microscopes. The continuum approach is also inadequate to analyse core-shell interactions at the atomic level. In result of this, we decided to complement the finite element modelling (FEM) with a molecular dynamics (MD) approach. In fact, modelling of filled carbon nanotubes mechanics has been traditionally carried out using mostly MD methods [20]. Moreover, MD uses well defined interatomic potentials which carry the physical nature of interatomic interactions, e.g. a response of a group of atoms to applied loads. With a well designed and tested potential, one obtains more accurate results (moreover, with atomic resolution) than with bulk continuum description using elastic properties such as Young's modulus or Poisson ratio.

In this work, MD simulations were carried out with the aim to analyse the mechanical behaviour of empty and ZnS-filled SWCNT subjected to an axial compressive loading. Furthermore, predictions for some relevant properties are made such as the Young's modulus, buckling critical force and strain.

2. Methods

The LAMMPS package [21] was used to study the ZnS@SWCNT system's mechanical response as a function of several length/diameter (L/D) ratios. Filled and empty zigzag SWCNT were modelled with diameters of 1 nm (13,0), 2 nm (26,0), 3 nm (38,0), 4 nm (51,0) and 5 nm (64,0), and lengths varying between 10 nm and 50 nm, bringing the total number of modelled CNT to 50. In MD, the interaction between atoms is defined by interatomic potentials which simulate the force fields between atoms through potential energy vs. interatomic distance laws [22]. In this work, the atomic pair interaction between C-C atoms and the forces acting between each atom of the confined ZnS nanowire were described by Tersoff potentials [23] (**Equations S1** to **S8** of the supplementary information). For the II-VI semiconductor, a diamond structure was adopted with a lattice parameter of 5.42 Å, using the potential parameterization defined in [24]. This pair potential allowed modelling of the inserted nanowire as a homogeneous crystal, replacing the Zn and S components by a single-type hypothetical average atom. The [001] crystal axis of ZnS was oriented along the SWCNT axis.

The C-ZnS interaction was described using the Lennard-Jones potential (L-J) [25] which provides an approximate description of the van der Waals interactions. Since no previous studies about L-J potential parameterisations for C-ZnS interactions were found, the Lorentz-Berthelot mixing rules [26, 27] were used to determine the vdW interaction parameters ($\varepsilon_{C\text{-}ZnS}$ and $\sigma_{C\text{-}ZnS}$). These rules are widely used and can be applied if the L-J parameters ε and σ are known for C-C and ZnS-ZnS interactions (Lorentz and Berthelot rules are given by the **Equations 1** and **2**, respectively).

$$\sigma_{ij} = \frac{\sigma_{ii} + \sigma_{jj}}{2} \tag{1}$$

$$\varepsilon_{ij} = \sqrt{\varepsilon_{ii}\varepsilon_{jj}} \tag{2}$$

The vdW interaction parameters for C-C and ZnS-ZnS were taken from [28] and [29], respectively, and are listed in **Table 1**. To save computational time, we truncated the L-J potential at the commonly used cut-off distance (r_c) of ≈ 2.5σ.

Table 1. Lennard-Jones parameters used to define C-ZnS interaction.

Interaction	ε (eV)	σ (Å)
C-C	4.57×10^{-3}	3.85
ZnS-ZnS	4.16×10^{-2}	2.50
C-ZnS	$\mathbf{1.27 \times 10^{-2}}$	**3.15**

Despite of their wide use, some authors have reported the Lorentz-Berthelot rules as inaccurate to predict vdW interactions [30]. Kong mixing rules [31] were therefore used as an alternative for more accurate results [30]. The calculations were performed for the same 50 models using also the Kong mixing rules. It turns out that the obtained results are very similar to Lorrentz-Berthelot ones and consequently we present them only in the supplemental material (**Tables S19** and **S22**).

Further information on the Tersoff parameters as well as the Lennard-Jones potential formulation and respective parameters can be found in the Supplementary Material. Further to this, we also include details concerning the calculation of the C-C equilibrium bond length and the ZnS equilibrium lattice parameter.

The SWCNT uniaxial compression was modelled by creating a rigid zone at both tips and moving one towards the other along the tube axis. The loading was applied at a rate of 0.001 nm/ps until strain values of at least 5% were reached. This resulted in a total number of time steps between 250,000 and 1,250,000 (for L = 10 nm and 50 nm, respectively). The temperature was maintained at a constant value of 0.1 K. Before applying the uniaxial loading, the nanotubes were relaxed for 20 ps.

3. Results and Discussion

We performed force versus displacement analysis for 50 different SWCNT models. The resulting data set was sufficiently large to identify several relationships linking buckling force, buckling strain and Young's modulus with the SWCNT length, diameter and aspect ratio.

Some examples of force vs. axial strain curves are plotted in **Figure 1**. These relate to empty (13,0), (26,0) and (51,0) nanotubes and their corresponding filled counterparts. All SWCNT were 20 nm long. At first glance, the comparison of empty and filled SWCNT curves suggests that the inner filling barely affects the slopes in the proportionality interval (elastic regime). Hence, encapsulation of the ZnS does not change significantly the axial stiffness (EA). This is an understandable

observation given the fact that the C shell has a much larger Young's modulus than the core ZnS nanowire (approximate theoretical values of 1000 GPa [32] and 100 GPa [33]). On the other hand, an increase of the critical buckling force and strain is noticeable for filled tubes, which is directly related to the stability increase provided by the II-VI semiconductor and its van der Waals interaction with the carbon wall. In fact, as known from bars theory, for a sufficiently long tube, the higher the sectional inertia, the higher is the force needed to reach buckling [34].

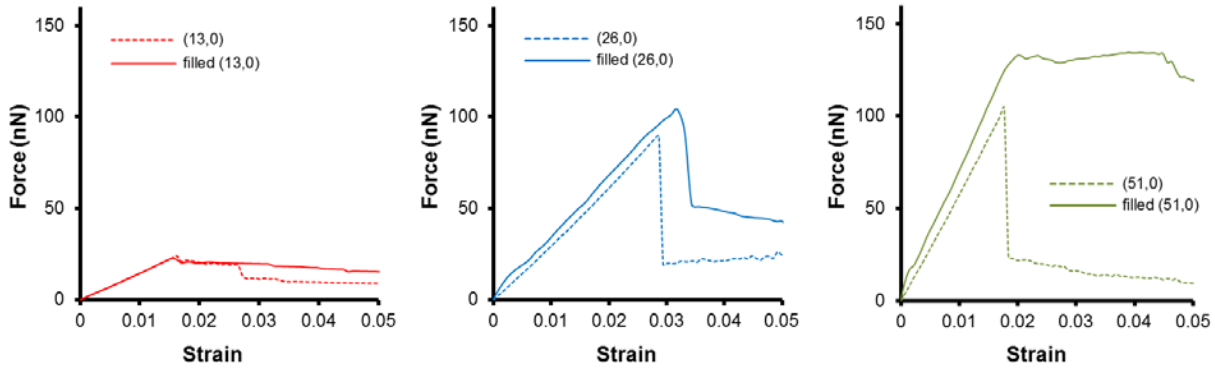

Figure 1. Predicted curves for compression force vs. axial strain for empty and filled (13,0), (26,0) and (51,0) SWCNT, all with a length of 20 nm. The thinner lines correspond to the empty nanotubes whereas the thicker ones relate to the filled cases.

Besides the above, a collapse mode and critical buckling force difference between empty and filled SWCNT was found to be related with the aspect ratio. Analysing the behaviour of the larger (51,0) SWCNT (with an aspect ratio of 5), an abrupt collapse was noticed for the empty model whereas the filled one showed a more ductile collapse (the internal axial force decreases smoothly). For an aspect ratio of 10 (represented by the (26,0) nanotube in **Figure 1**), both empty and filled cases were concordant. Here, an abrupt collapse was noticed meaning that the axial force increases linearly with strain until the tube suddenly buckles at the critical strain. Lastly, for an aspect ratio of 20, both empty and filled (13,0) SWCNT showed first an elastic response reaching small yield strains, followed by an almost constant residual force.

The collapse under compressive force of an empty and filled (26,0) SWCNT is illustrated in **Figure 2**. Four different stages are highlighted, namely, **I**) the initial, relaxed configuration, **II**) the system just before it buckles, **III**) immediately after the structural collapse and **IV**) the final, fully compressed configuration obtained at 10% strain. A similar buckling behaviour was recently reported from Monte Carlo simulations also for applied hydrostatic pressure [35]. The higher

deformability of the empty SWCNT seen in **Figure 2** provides a clear visual clue of how the yield strength is increased with the inclusion of the ZnS.

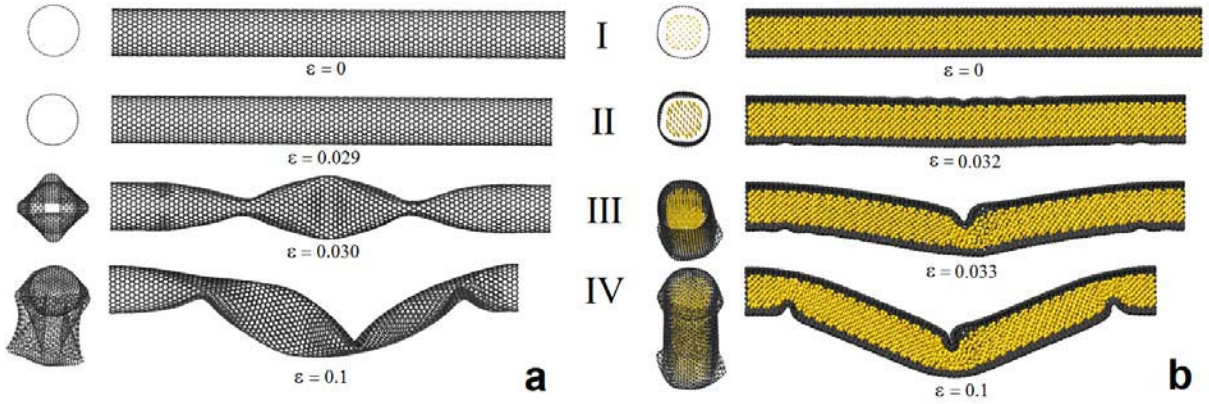

Figure 2. Snapshots of the deformation process of a 20 nm long (26,0) SWCNT in the (a) empty and (b) filled states. The yellow domains in (b) represent the confined ZnS nanowire.

In the next sections, we will describe more quantitatively how properties such as the buckling force and strain are affected by the inclusion of the ZnS.

3.1 Young's modulus

Applying Hooke's law (3) combined with the expression that defines stress in a specific section under axial strain (4) and the definition of axial strain (5), the Young's modulus can be expressed through (6) using the modelled force-strain data.

(3)

– (4)

— (5)

——— (6)

where σ represents stress, ε denotes strain, A is the cross-sectional area of the tube, L refers the length and ΔL the elongation. Considerable inconsistency has been found in the literature regarding the definition of the effective thickness of the SWCNT [36] (from 0.062 nm [37] to 0.69 nm [38]). In the specific case of the empty tubes, this discrepancy directly affects the definition of the cross

sectional area which in turn drastically influences the calculation of the Young's modulus. To minimise this uncertainty, we adopted a different approach where we considered the perimeter, πD, instead of the cross-sectional area of the carbon shell. As a result we obtained a "linear Young's modulus" (E_{linear}), corresponding to a unit thickness of the host wall and expressed by (7). In this way, one can estimate the Young's modulus when provided with a specific effective thickness value of the carbon layer. It should be noted that this approach applies to empty tubes only.

_____ (7)

When the values calculated using (7) are divided by the wall thickness adopted, SWCNT effective Young's modulus (E) is obtained. E_{linear} is plotted as a function of the zigzag SWCNT diameter in **Figure 3** and presented in **Table S16** in Supplementary Material. Here, a range of lengths was considered (within the interval of 10 to 50 nm) for each (n,m) nanotube.

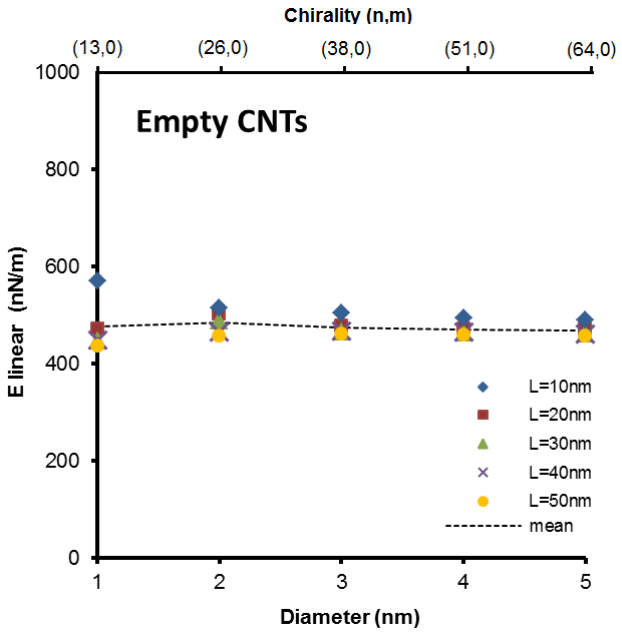

Figure 3. E_{linear} vs. diameter for all empty SWCNT length analysed adopting a unit thickness.

Within the length interval analysed, **Figure 3** shows that the E_{linear} for the larger empty tubes converged to an average value of ~470 nN/nm. The exception was the shortest (13,0) that, at 10 nm length, resulted in a E_{linear} of 570 nN/m.

The uncertainty derived from the definition of the wall thickness for the carbon shell is irrelevant in the case of filled sections. Notwithstanding, for hybrid elements, the Young's modulus becomes a

property of a specific cross section, since it depends on the ratio of the section components (ZnS and C, in the present case). It is straightforward that the greater the proportion of ZnS, the lower is the Young's modulus of the tube. The comparison between each hybrid filled SWCNT Young's Modulus is therefore meaningless and, hence, this analysis was not made in the present work.

3.2 Buckling force

Two different failure modes were observed in the present study. Interestingly, both were present in the empty and filled configurations (albeit in lesser degree in the ZnS-filled nanotubes). The first, i.e. Mode 1, is due to local buckling effects [39] that occur punctually in the carbon shell (**Figures 4a and 4b**). The second mode (Mode 2) refers to the global structural instability of the nanotubes when compressed uniaxially, as shown in **Figure 4c**. This figure exemplifies the typical global curvature shape of a bi-clamped long element.

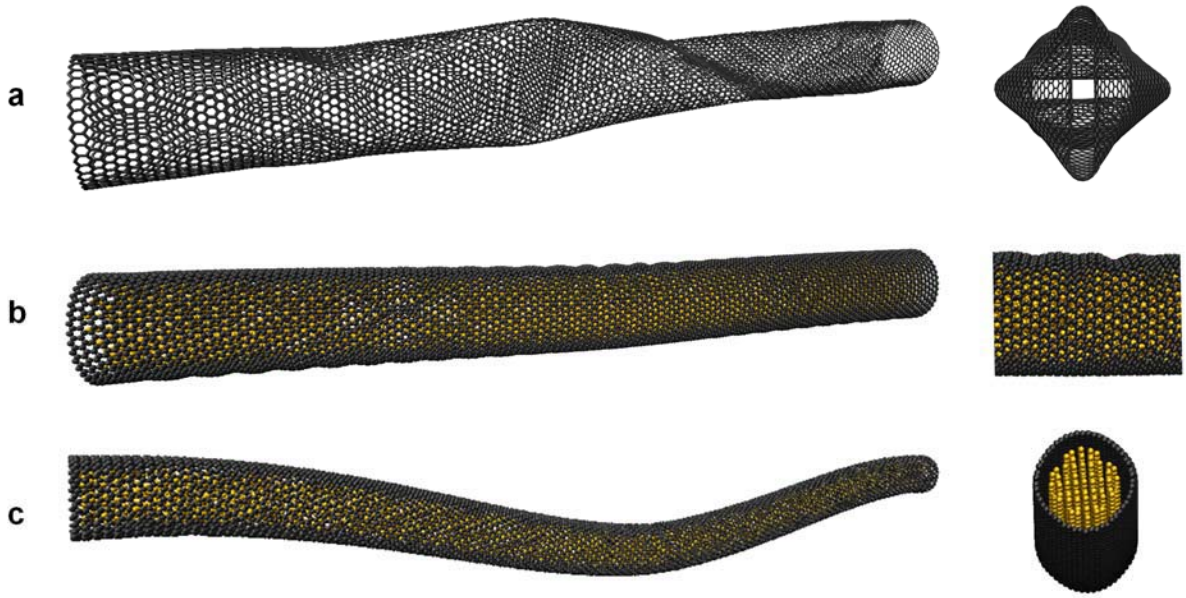

Figure 4. Illustration of the observed buckling modes. a) Mode 1 for a hollow (38,0) SWCNT and 30 nm long; b) Mode 1 for a filled (38,0) SWCNT and 30 nm long; c) Mode 2 for a filled (26,0) SWCNT and 40 nm long.

Although the buckling modes are common to all nanotubes analysed, the critical forces involved may differ. Analysing the compression process, a clearly smaller buckling resistance was noticed for the longest tubes. Such fact led us to conclude that the resistance of SWCNT under axial

compression is also influenced by the tube length and not only by the cross-sectional geometry. In fact, the length behavioural dependence is widely acknowledged in the classical mechanics of columnar materials which predict that, as a consequence of their initial shape, long nanotubes would deform in the Euler-type mode (here, Mode 2) [34]. Thus, if we consider the buckling of an ideal column (i.e. initially straight, axially loaded), and if this is sufficiently long, i.e., the effective length (L_{ef}) is greater than the critical length (L_{cr}), it will buckle at the critical yield force (P_{cr}), without any relation to the critical stress of the material (σ_{cr}). Then, by reducing the length, Mode 1 takes over Mode 2. The typical yield force values, defined by Euler, of doubly clamped tubes (L_{ef} = 0.5L) subjected to axial compression, as a function of the element length [34], is defined by Eq. 8 and 9 for hollow tubes and Eq. 10 and 11 for filled tubes.

$$P_{cr} = A_c \sigma_{cr,c} \quad \text{and} \quad L_{ef} \leq L_{cr} \tag{8}$$

$$P_{cr} = \frac{\pi^2}{0.5L^2} E_c \frac{\pi}{4} (r_{out}^4 - r_{int}^4) \quad \text{and} \quad L_{ef} \geq L_{cr} \tag{9}$$

$$P_{cr} = A_c \sigma_{cr,c} + A_{ZnS} \sigma_{cr,ZnS} \quad \text{and} \quad L_{ef} \leq L_{cr} \tag{10}$$

$$P_{cr} = \frac{\pi^2}{0.5L^2} \frac{\pi}{4} [E_c (r_{out}^4 - r_{int}^4) + E_{ZnS}\, r_{int}^4] \quad \text{and} \quad L_{ef} \geq L_{cr} \tag{11}$$

In fact, it is possible to make an association between the critical buckling force (extracted from **Figure 1**) and the dimensions of the nanotubes (diameter and length) as plotted in **Figures 5a and 5b** for the empty and filled cases, respectively. While the ensemble of the shortest 10 nm empty nanotubes showed a relatively constant critical buckling force, the remaining cases followed a similar asymptotic trend whereby the critical buckling force increases with diameter up to a similar threshold (**Figure 5a**). The convergence point is attained at 5 nm diameter for all lengths analysed with an average buckling force of 102 nN. An averaged curve (dashed line) is also added to the plot for guidance.

A similar behaviour was found for the filled SWCNT (**Figure 5b**). Interestingly, the shortest nanotube also followed the trend common to all other lengths. Again, there is a convergence towards a common buckling force, although it happened right from 4 nm diameters and shows a decreasing trend until the largest diameter analysed. The average buckling force of 4 nm diameter filled SWCNT was approximately 132 nN vs. 124 nN for the 5 nm diameter. The comparison of the average curves obtained in **Figures 5a** and **5b** demonstrate well the enhancement of the buckling force due to the filling. As an example, the average buckling force increment for the (51,0) SWCNT was 34%.

It is well known from tubes' applied mechanics [40] that the critical force of a tube under axial compression depends not only of its cross section dimensions, but also of its length and support conditions. According to these mechanical laws, from a certain value of slenderness ratio, the behaviour of columnar elements is also dependent of their L_{ef} defined through the initial length and support condition of each tip. Hereupon, it is understandable that for the same cross section, the buckling force of a SWCNT varies with the L_{ef}. Looking at the plots of **Figures 5a** and **5b**, it is evident that from a certain diameter onwards, the length of the tubes no longer influences significantly their buckling force.

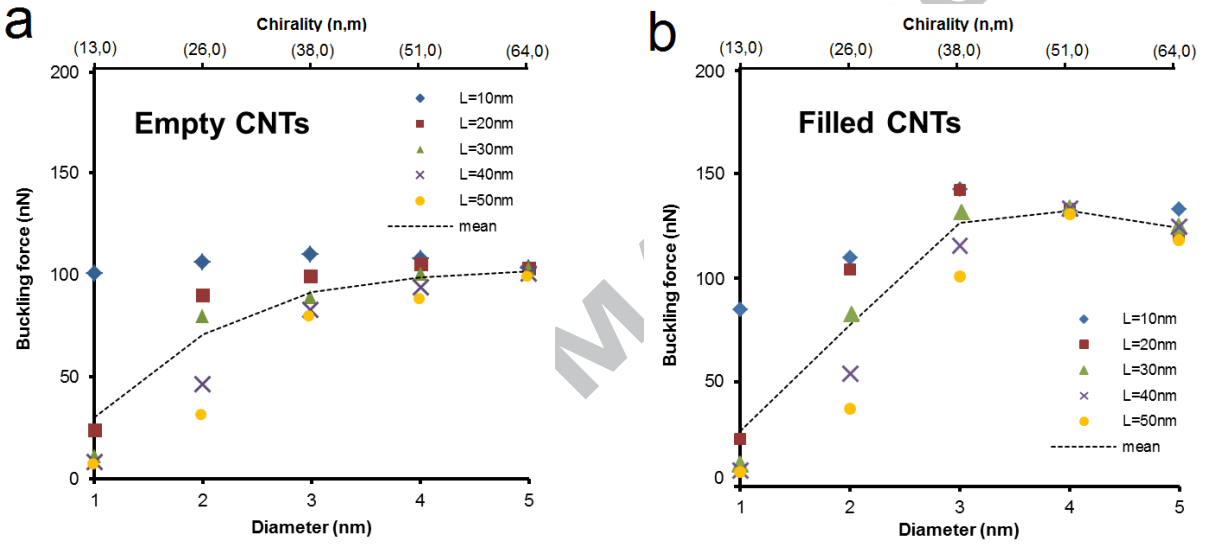

Figure 5. Buckling force vs. diameter for all SWCNT lengths. a) empty nanotubes, b) filled nanotubes.

Given the influence of both length and diameter of the nanotube in the critical buckling force it is more useful to use the aspect ratio (L/D) to understand the relationship between dimensions and failure modes.

Figures 6a and **6b** show the relation of L/D and buckling force for empty and filled nanotubes, respectively. In both plots, the filled markers represent the SWCNT where Mode 1 of failure (local buckling) dominates while the hollow markers correspond to those cases where Mode 2 is predominantly observed (global buckling). Two phenomena are evident from inspection of the plots. First, the buckling force decreases with increasing aspect ratio, as expected. Second, there is a critical value of L/D ratio which separates the regions where Modes 1 and 2 dominate. For the

empty SWCNT (**Figure 6a**), this critical value is 17-20, i.e., all nanotubes with aspect ratio larger than 17 will deform via Mode 2. For the filled SWCNT (**Figure 6b**), this limit is lower, 10-12.

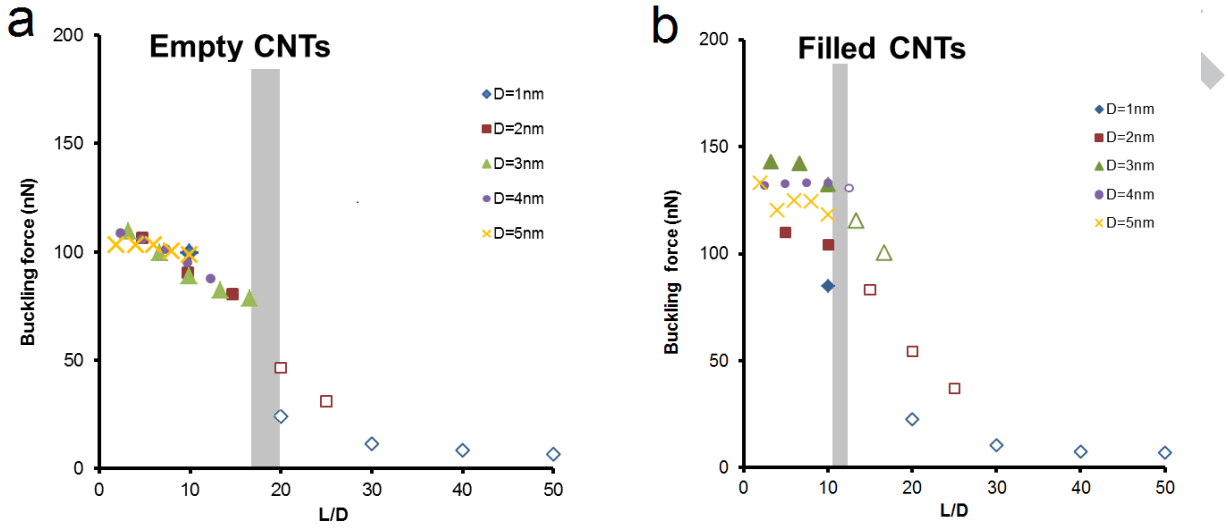

Figure 6. Buckling force vs. aspect ratio plots for all the tested SWCNT. a) empty SWCNT; b) filled SWCNT. In both plots, the grey stripes show the L/D range corresponding to the transition between Mode 1 and Mode 2 of buckling.

3.3 Buckling strain

Just as for the critical buckling force, the above analysis can be performed for the yield strain, enabling us to understand how the SWCNT dimensions influence their final yield strain. **Figures 7a** (empty SWCNT) and **7b** (filled SWCNT) show the buckling strain as a function of the nanotubes' diameter for the five lengths analysed (10, 20, 30, 40 and 50 nm). With the exception of the nanotube with the smallest diameter (1 nm) and shortest length (10 nm), there was an initial increase of critical strain peaking at 2 nm and 3 nm diameter, respectively for the empty and filled structures. Thereafter, the empty structures have similar buckling strains for all lengths, a trend that converges to an average value of 1.4% for the largest nanotube analysed. The same occurs with filled tubes, despite of a less pronounced trend, leading to a strain average value of 1.7% for the 5 nm diameter SWCNT.

The discrepant high critical strain observed for the empty 1 nm x 10 nm SWCNT (0.055, **Figure 7a**) was also obtained for its filled counterpart (0.048, **Figure 7b**). Interestingly, the narrowest nanotubes (diameter of 1 nm) showed an opposite behaviour than expected. In fact, the buckling

strain is lower for the filled carbon shells as opposed to the empty ones. Contrastingly, the buckling strain enhancement for the largest filled nanotubes (diameters of 4 and 5 nm) was of ≈21% with respect to the corresponding empty SWCNT.

As can be noticed from **Figure 2b II** and **2b III**, the local buckling or shell-like buckling of the empty and filled tubes (Mode 1) is associated with the formation of waves in the structure of the carbon layer. As expected, such a buckling occurs for empty SWCNTs associated with smaller wave numbers than for filled SWCNTs but with greater wave length at a lower strain rate [41].

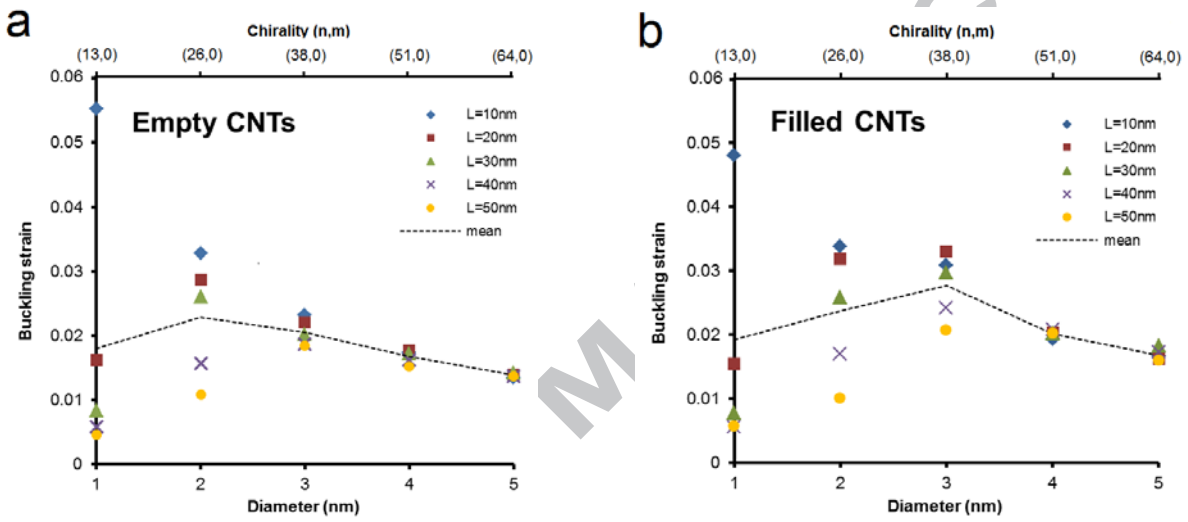

Figure 7. Buckling strain vs. diameter for all SWCNT lengths. a) empty nanotubes, b) filled nanotubes.

Finally, the critical strain of each nanotube was plotted as a function of its aspect ratio, as demonstrated in **Figures 8a** and **8b**. Both failure modes described above are represented with filled and hollow markers for buckling Modes 1 and 2, respectively. Here the change between the dominant modes does not appear as abrupt as in the case of the buckling force. An interesting observation is that for both SWCNT configurations there seems to be no relationship between L/D and buckling strain, particularly when comparing the results of the five cases where the buckling Mode 1 is dominant. On the other hand, when the tubes buckle according to Mode 2 (hollow markers), the behaviour of the empty and filled SWCNT is coincident irrespective of the diameters considered. Overall, one can conclude that beyond a certain level of slenderness ratio, the buckling strain of empty and filled tubes can be expressed as a function of their L/D ratio using a universal curve.

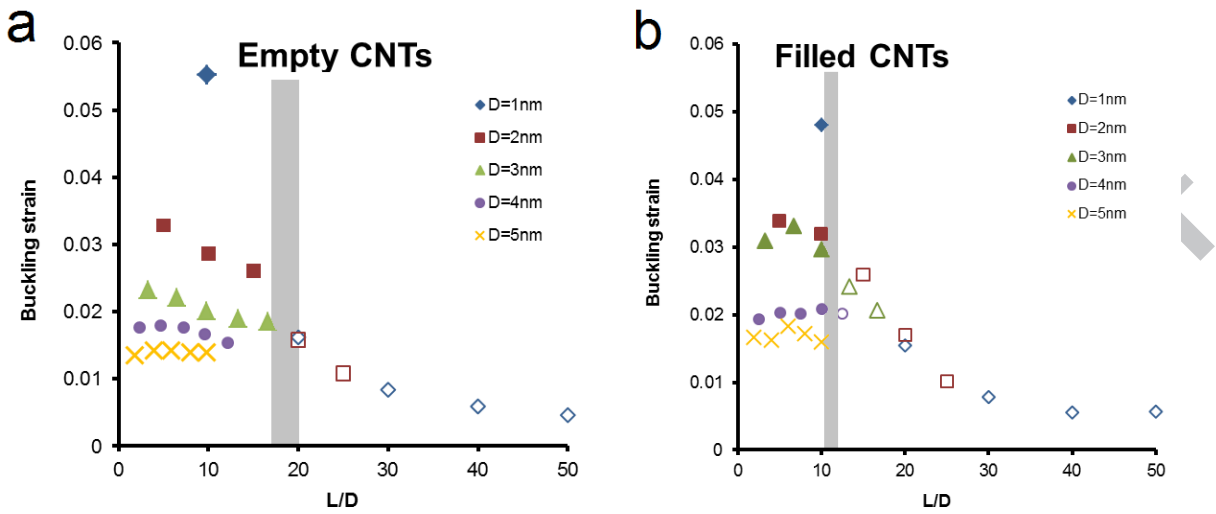

Figure 8. Buckling strain vs. aspect ratio plots for all the tested SWCNT. a) empty SWCNT; b) filled SWCNT. In both plots, the grey stripes show the L/D range which defines the transition between Mode 1 and Mode 2 of buckling.

3.4 Comparison with existing results

Today, there is a wealth of information on the mechanics of empty CNTs. By contrast, there are relatively few studies that have focused on the mechanical properties and response of filled CNTs. As highlighted in [20], the uniaxial buckling of SWCNTs filled with molecular or elemental substances (e.g. He [42], Ne [43], CH_4 [43], C_{20} [44], C_{36} [44], C_{60} [44, 45] and Au [46]) was studied using armchair nanotubes, exclusively. These have dissimilar responses to the present zigzag structures which, added to the different conditions specified by each team (e.g. support, temperature or potentials), makes a direct comparison difficult. Notwithstanding, **Table S23** brings together all the results found in the literature for compression experiments on filled SWCNT using MD simulations.

4. Conclusions

Employing classical molecular dynamics, we investigated the mechanical properties related to uniaxial compression of SWCNT filled with ZnS nanowires for a wide range of diameters and lengths, and studied the influence of each parameter on buckling force and strain. The inner filling is shown to affect rather weakly the axial rigidity of the nanotubes. Nonetheless, it led to important enhancements of other properties. Amongst these are the increased buckling force and strain due to

the gain in stiffness provided by the filling. In other words, the nanotubes become more stable when loaded (34% and 21% of average gain of critical buckling force and strain, respectively, considering 50 nm diameter nanotubes). It was also verified that, besides the cross sectional area, the length of the SWCNT also influences the buckling force. For both filled and empty configurations, two different buckling modes were seen (local and global buckling). Interestingly, a critical value of L/D defining the limit between the first (local) buckling mode and the second (global) one could be determined. Despite a global stability enhancement, this L/D value was lower for the filled tubes than for the hollow ones. Lastly, it should be noticed that nanotubes with D = 1 nm and L = 10 nm often possess qualitatively different behaviour from the rest of our models. This is particularly important as a number of MD papers on the subject have typically adopted similar dimensions (see [20] for a review). The present work contributes to the development of nanopippettes based on carbon nanotubes as it demonstrates that the mechanics of these systems may be used as independent, non-visual markers for a filled versus empty configuration comparison.

Acknowledgement:

We acknowledge financial support from the COMPETE-FEDER program and FCT to the projects PTDC/EME-PME/112073/2009 and PEst-C/CTM/LA0011/2011. This work was partially funded by KAUST. AM is grateful to the Da Vinci program for an internship scholarship. We thank the reviewers for their constructive suggestions.

References

1. D. Ugarte, T. Stöckli, J.M. Bonard, A. Châtelain, and W.A. Heer, *Filling carbon nanotubes.* Applied Physics A, 1998. **67**: p. 101-105.

2. P.M. Ajayan and S. Iijima, *Capillarity-induced filling of carbon nanotubes.* Nature, 1993. **361**(6410): p. 333-334.

3. K. Cho, X. Wang, S. Nie, Z. Chen, and D.M. Shin, *Therapeutic nanoparticles for drug delivery in cancer.* Clinical Cancer Research, 2008. **14**(5): p. 1310-1316.

4. Z. Liu, K. Chen, C. Davis, S. Sherlock, Q. Cao, X. Chen, et al., *Drug delivery with carbon nanotubes for in vivo cancer treatment.* Cancer Research, 2008. **68**(16): p. 6652-6660.

5. E. Dervishi, Z. Li, Y. Xu, V. Saini, A.R. Biris, D. Lupu, et al., *Carbon Nanotubes: Synthesis, Properties, and Applications.* Particulate Science and Technology, 2009. **27**(2): p. 107-125.

6. M. Arlt, D. Haase, S. Hampel, S. Oswald, A. Bachmatiuk, R. Klingeler, et al., *Delivery of carboplatin by carbon-based nanocontainers mediates increased cancer cell death.* Nanotechnology, 2010. **21**(33): p. 335101.

7. J.P. Tessonnier, G. Wine, C. Estournes, C. Leuvrey, M.J. Ledoux, and C. Pham-Huu, *Carbon nanotubes as a 1D template for the synthesis of air sensitive materials: About the confinement effect.* Catalysis Today, 2005. **102-103**: p. 29-33.

8. P.M.F.J. Costa, U.K. Gautam, Y. Bando, and D. Golberg, *The electrical delivery of a sublimable II–VI compound by vapor transport in carbon nanotubes.* Carbon, 2011. **49**(12): p. 3747-3754.

9. K. Svensson, H. Olin, and E. Olsson, *Nanopipettes for Metal Transport.* Physical Review Letters, 2004. **93**(14): p. 145901.

10. P.M.F.J. Costa, U.K. Gautam, Y. Bando, and D. Golberg, *Comparative study of the stability of sulfide materials encapsulated in and expelled from multi-walled carbon nanotube capsules.* Carbon, 2011. **49**(1): p. 342-346.

11. P.M.F.J. Costa, T.W. Hansen, J.B. Wagner, and R.E. Dunin-Borkowski, *Imaging the Oxidation of ZnS Encapsulated in Carbon Nanotubes.* Chemistry – A European Journal, 2010. **16**(39): p. 11809-11812.

12. P.M.F.J. Costa, U.K. Gautam, Y. Bando, and D. Golberg, *Direct imaging of Joule heating dynamics and temperature profiling inside a carbon nanotube interconnect.* Nature Communications, 2011. **2**(1).

13. P.M.F.J. Costa, U.K. Gautam, Y. Bando, and D. Golberg, *Effect of Electron Beam Irradiation and Heating on the Structural Stability of Sulphide-Filled Carbon Nanotubes.* Microscopy and Microanalysis, 2012. **18**(SupplementS5): p. 77-78.

14. P.M.F.J. Costa, U.K. Gautam, M. Wang, Y. Bando, and D. Golberg, *Effect of crystalline filling on the mechanical response of carbon nanotubes.* Carbon, 2008. **47**(2): p. 541-544.

15. A.O. Monteiro, P.M.F.J. Costa, and P.B. Cachim, *Finite element modelling of the mechanics of discrete carbon nanotubes filled with ZnS and comparison with experimental observations.* Journal of Materials Science, 2014. **49**(2): p. 648-653.

16. P.M.F.J. Costa, P.B. Cachim, U.K. Gautam, Y. Bando, and D. Golberg, *The mechanical response of turbostratic carbon nanotubes filled with Ga-doped ZnS: I. Data processing for the extraction of the elastic modulus.* Nanotechnology, 2009. **20**(40).

17. P.M.F.J. Costa, P.B. Cachim, U.K. Gautam, Y. Bando, and D. Golberg, *The mechanical response of turbostratic carbon nanotubes filled with Ga-doped ZnS: II. Slenderness ratio and crystalline filling effects.* Nanotechnology, 2009. **20**(40).

18. D. Golberg, P.M.F.J. Costa, M.-S. Wang, X. Wei, D.-M. Tang, Z. Xu, et al., *Nanomaterial Engineering and Property Studies in a Transmission Electron Microscope.* Advanced Materials, 2012. **24**(2): p. 177-194.

19. P.M.F.J. Costa, P.B. Cachim, U.K. Gautam, Y. Bando, and D. Golberg, *The mechanical response of turbostratic carbon nanotubes filled with Ga-doped ZnS: II. Slenderness ratio and crystalline filling effects.* Nanotechnology, 2009. **20**(40): p. 405707.

20. A.O. Monteiro, P.B. Cachim, and P.M.F.J. Costa, *Mechanics of filled carbon nanotubes.* Diamond and Related Materials, 2014. **44**: p. 11-25.

21. S. Plimpton, *Fast Parallel Algorithms for Short-Range Molecular Dynamics.* Journal of Computational Physics, 1995. **117**(1): p. 1-19.

22. J. Lee, G., *Computational Materials Science,* 2011, USA: CRC Press.

23. J. Tersoff, *Modeling solid-state chemistry: Interatomic potentials for multicomponent systems.* Physical Review B, 1989. **39**(8): p. 5566-5568.

24. F. Benkabou, H. Aourag, and M. Certier, *Atomistic study of zinc-blende CdS, CdSe, ZnS, and ZnSe from molecular dynamics.* Materials Chemistry and Physics, 2000. **66**(1): p. 10-16.

25. J.E. Lennard Jones, *On the Determination of Molecular Fields. II. From the Equation of State of a Gas.* Proceedings of the Royal Society of London, 1924. **106**(738): p. 463-477.

26. H.A. Lorentz, *Ueber die Anwendung des Satzes vom Virial in der kinetischen Theorie der Gase.* Annalen der Physik, 1881. **248**(1): p. 127-136.

27. D. Berthelot, *Sur le Mélange des Gaz.* Compt. Rendus (Bachelier Paris), 1898. **126**: p. 1703-1706.

28. A.K. Rappe, C.J. Casewit, K.S. Colwell, W.A. Goddard, and W.M. Skiff, *UFF, a full periodic table force field for molecular mechanics and molecular dynamics simulations.* Journal of the American Chemical Society, 1992. **114**(25): p. 10024-10035.

29. M. Grünwald, A. Zayak, J.B. Neaton, P.L. Geissler, and E. Rabani, *Transferable pair potentials for CdS and ZnS crystals.* The Journal of Chemical Physics, 2012. **136**(23): p. -.

30. J. Delhommelle and P. MilliÉ, *Inadequacy of the Lorentz-Berthelot combining rules for accurate predictions of equilibrium properties by molecular simulation.* Molecular Physics, 2001. **99**(8): p. 619-625.

31. C.L. Kong, *Combining rules for intermolecular potential parameters. II. Rules for the Lennard-Jones (12–6) potential and the Morse potential.* The Journal of Chemical Physics, 1973. **59**(5): p. 2464-2467.

32. M.-F. Yu, B.S. Files, S. Arepalli, and R.S. Ruoff, *Tensile Loading of Ropes of Single Wall Carbon Nanotubes and their Mechanical Properties.* Physical Review Letters, 2000. **84**(24): p. 5552-5555.

33. U. Rössler, *ZnS: elastic constants, internal-strain parameter*, 2013, Springer Berlin Heidelberg. p. 198-201.

34. S. Timoshenko and J. Gere, *Theory of elastic stability,* 1961, USA: McGraw-Hill.

35. Y.W. Sun, D.J. Dunstan, M.A. Hartmann, and D. Holec, *Nanomechanics of Carbon Nanotubes.* PAMM, 2013. **13**(1): p. 7-10.

36. C.Y. Wang and L.C. Zhang, *A critical assessment of the elastic properties and effective wall thickness of single-walled carbon nanotubes.* Nanotechnology, 2008. **19**(7): p. 075705.

37. T. Vodenitcharova and L. Zhang, *Effective wall thickness of a single-walled carbon nanotube.* Physical Review B, 2003. **68**(16).

38. G.M. Odegard, T.S. Gates, L.M. Nicholson, and K.E. Wise, *Equivalent-continuum modeling of nano-structured materials.* Composites Science and Technology, 2002. **62**(14): p. 1869-1880.

39. C.Q. Ru, *Effective bending stiffness of carbon nanotubes.* Physical Review B, 2000. **62**(15): p. 9973-9976.

40. S.B. Batdorf, M. Schildcrout, and M. Stein, *Critical Stress of Thin-Walled Cylinders in Axial Compression* 1947, National Advisory Comittee For Aeronotics: Washington. p. 21.

41. D.R. Siddle and D.J. Dunstan, *Buckling of compressively strained epitaxial crystal structures.* Philosophical Magazine A, 1994. **70**(2): p. 233-246.

42. K. Xia, Z.Y. Pan, B.E. Zhu, Y. Xiao, and Y.X. Wang, *Effect of filling He on the buckling force of host single-walled carbon nanotube.* International Journal of Modern Physics B, 2010. **24**(17): p. 3373-3382.

43. B. Ni, S.B. Sinnott, P.T. Mikulski, and J.A. Harrison, *Compression of carbon nanotubes filled with C60, CH4, or Ne: Predictions from molecular dynamics simulations.* Physical Review Letters, 2002. **88**(20): p. 2055051-2055054.

44. Z.X. ZHANG, Z.Y. PAN, Q. WEI, Z.J. LI, L.K. ZANG, and Y.X. WANG, *Mechanics of Nanotubes filled with C60, C36 and C20.* International Journal of Modern Physics B, 2003. **17**(26): p. 4667-4674.

45. L. Zhou, B.E. Zhu, Z.Y. Pan, Y.X. Wang, and J. Zhu, *Reduction of the buckling strength of carbon nanotubes resulting from encapsulation of C60 fullerenes.* Nanotechnology, 2007. **18**(27): p. 275709.

46. S.H. Guo, B.E. Zhu, X.D. Ou, Z.Y. Pan, and Y.X. Wang, *Deformation of gold-filled single-walled carbon nanotubes under axial compression.* Carbon, 2010. **48**(14): p. 4129-4135.